Numerical Analysis of Mixing of Nonequilibrium Supersonic Flows

D. Zeitoun,* M. Maurel,† M. Imbert,‡ and R. Brun§
Université de Provence, Marseille, France

The flowfield of a CO_2-N_2 mixing gasdynamic laser is numerically analyzed by using laminar, two-dimensional unsteady Navier-Stokes equations coupled with the appropriate relaxation equations describing the vibrational transfer between the internal modes. These equations result from an averaging through the third dimension in order to take into account the area increase of the laser cavity in this direction. The equation system is solved with an explicit, time-dependent, second-order finite-difference technique. The flowfield in each nozzle where CO_2 and N_2 are premixed and the main laser cavity are described. The analysis shows the complex structure of the flowfield and the influence of the premixing zone and the diverging section on the small-signal gain coefficients and the evolution of the flow quantities.

Nomenclature

A	= cavity area
C_v	= specific heat at constant volume
D_{km}	= diffusion coefficient
E	= total energy per unit mass
e_{v_i}	= vibrational energy per unit mass of species i
$\boldsymbol{F},\boldsymbol{G}$	= flux vectors
H	= centerline distance
$\boldsymbol{H}$	= source vector
h_k	= heat of formation of species k
k_m	= conductivity coefficient of the mixture
L_x,L_y	= one-dimensional operators
Le_v	= vibrational Lewis number
P	= static pressure
Pr_v	= vibrational Prandtl number
q_{vix},q_{viy}	= Cartesian heat vibrational flux components
q_x,q_y	= Cartesian heat flux components
T	= temperature of the mixture
T_v	= vibrational temperature
t	= time coordinate
$\boldsymbol{U}$	= conserved quantity vector
u, v	= Cartesian velocity components
x,y,z	= Cartesian coordinates
Y_k	= mass fraction of species k
Δt	= step time integration
λ_m	= second coefficient of viscosity, $-2/3\mu_m$
μ_m	= shear viscosity of the mixture
ν_1,ν_2,ν_3	= vibrational modes of CO_2
ν_4	= vibrational mode of N_2
ρ	= density of the mixture
ρ_k	= density of species k
$\tau_{xx},\tau_{yy},\tau_{xy}$	= stress tensor components
$\dot{\omega}_i$	= source terms

Subscripts

i	= vibrational mode of species
j	= reactive species
k	= species
m	= mixture
o	= reservoir condition
s	= total species number

Superscripts

n	= nth level in time
*	= excited N_2 molecules

Received July 10, 1989; revision received Jan. 3, 1990.

*Professor, Department Milieux Hors d'Equilibre, Laboratoire S.E.T.T.
†Graduate Student, Laboratoire S.E.T.T.
‡Maître de Conférence, Laboratoire S.E.T.T.
§Head of the Department, Laboratoire S.E.T.T. Member AIAA.

Introduction

IT is well known that lasing effects are obtained in media where atoms or molecules present population inversions in their energy modes and are contained in an optical resonator. The diversity of the laser sources comes from the different nature of the used active media and of the efficiency of the pumping processes maintaining the population inversion. The aim of the present paper is the analysis of a gasdynamic CO_2-N_2 laser. In this type of laser, the population inversion of the vibrational modes of the CO_2 molecules is obtained from the interaction between an excited nitrogen stream and a low-temperature CO_2-He jet.[1,2] During the mixing, there is a collisional transfer of vibrational energy between the excited N_2 gas and the highest internal mode of CO_2, which is, therefore, overpopulated. This active medium is then expanded before flowing into the cavity in which the laser effect is obtained by de-excitation of CO_2.

In order to increase the efficiency of the mixing, the gases are first expanded in small-dimension nozzles up to supersonic velocities. The pumping or inversion process is therefore obtained in two steps: excitation of the expanded N_2 gas and then transfer to the lasing CO_2 gas. The numerical simulation of this type of laser, a downstream mixing gasdynamic laser, in which the CO_2-N_2 mixing comes from two parallel nozzles representing one element of a bank of nozzles has been presented in many papers.[3-5] In these works, the nozzle boundary layers are generally neglected.

In the present study, the nozzles are staggered and a premixing between a nonequilibrium high-temperature N_2 flow and a cold CO_2/He/H_2/Ar jet is operated in one of the nozzles. This premixed flow is expanded before mixing again with an another CO_2/He/H_2/Ar jet in the laser cavity. Futhermore, in order to overexpand the jets and, therefore, to promote the energetic transfer, the cavity walls parallel to the optical beam diverge. The flowfield in each nozzle is calculated from the numerical integration of laminar two-dimensional Navier-Stokes equations averaged in the third direction, taking into

account the area increase of the cavity. The equations that govern the energy transfer process between the internal modes close the system. The numerical method is based on a predictor-corrector finite scheme with a time splitting technique.[6,7]

The details of the flowfield are obtained from the computation in the nozzles as well as in the cavity in which there is a wall angle of 5 deg. The results concern the development of the two mixing zones, the energetic transfers between the CO_2 and N_2 molecules, and their influence of the small gain coefficients along the cavity.

Governing Equations

The complete system of governing equations describing an unsteady three-dimensional viscous flow of a multicomponent nonequilibrium gas is integrated in the z directive in order to obtain an averaged two-dimensional set of equations. This set may be written in the following conservation form:

$$\frac{\partial U}{\partial t} + \frac{\partial F}{\partial x} + \frac{\partial G}{\partial y} + H = 0$$

where the $(K_{s-1} + 8)$ component fluxes are

$$U = A \begin{vmatrix} \rho_k & k = 1,\ldots, s-1 \text{ (for each species)} \\ \rho & \\ \rho u & \\ \rho v & \\ \rho E & \\ \rho_j e_{v_i} & j = (CO_2);\ j = 2\ (N_2) \\ & i = 1,2,3\ (v_1,v_2,v_3 \text{ of } CO_2);\ i = 4\ (N_2) \end{vmatrix}$$

$$F = A \begin{vmatrix} \rho_k u - \rho D_{km} \dfrac{\partial Y_k}{\partial x} \\ \rho u \\ \rho u^2 + P - \tau_{xx} \\ \rho uv - \tau_{xy} \\ (\rho E + P - \tau_{xx})u - v\tau_{xy} + q_x \\ \rho_j u e_{v_i} - \rho e_{v_i} D_{jm} (\partial Y_j/\partial x) + q_{v_{ix}} \end{vmatrix}$$

$$G = A \begin{vmatrix} \rho_k v - \rho D_{km} (\partial Y_k/\partial y) \\ \rho v \\ \rho uv + P - \tau_{xy} \\ \rho v^2 + P - \tau_{yy} \\ (\rho E + P - \tau_{yy})v - u\tau_{xy} + q_y \\ \rho_j v e_{v_i} - \rho e_{v_i} D_{jm} (\partial Y_j/\partial y) + q_{v_{iy}} \end{vmatrix}$$

The component source terms are

$$H = \begin{vmatrix} 0 \\ 0 \\ -(P + \tau_{xx}) \dfrac{dA}{dx} \\ +\tau_{yx} \dfrac{dA}{dx} \\ 0 \\ \rho_j \dot{\omega}_i A \end{vmatrix}$$

with

$$E = T\sum_k C_{v_k} Y_k + \sum_k Y_k e_{v_k} + 1/2\,(u^2 + v^2)$$

$$\tau_{xx} = (\lambda_m + 2\mu_m) \frac{\partial u}{\partial x} + \lambda_m \frac{\partial v}{\partial y}$$

$$\tau_{xy} = \mu_m \left(\frac{\partial u}{\partial y} + \frac{\partial v}{\partial x} \right)$$

$$\tau_{yy} = (\lambda_m + 2\mu_m) \frac{\partial v}{\partial y} + \lambda_m \frac{\partial u}{\partial x}$$

$$q = -k_m \nabla T - \sum_k (h_k + e_{v_k}) \rho D_{km} \nabla Y_k + q_v$$

$$q_v = -\sum_i \mu_m (Le_{v_j}/Pr_{v_j}) Y_j \nabla e_{v_i}$$

In these expressions, the transport coefficients are calculated from Wilke's law for the mixture viscosity[8] and from the empirical formula given by Chapman and Cowling for the binary diffusion coefficient D_{km}.[9] A detailed presentation of these equations may be found in Ref. 10. The vibrational Lewis and Prandtl numbers are chosen as follows

$Le_v = 1$ for CO_2 and N_2

$Pr_v = 0.72$ for N_2

$Pr_v = 0.66$ for CO_2

Vibrational Model

Because the CO_2 molecule is a linear triatomic molecule it possesses three vibrational modes that have a frequency ν_i, vibrational energy e_{v_i}, and corresponding temperature T_i $(i = 1,2,3)$. The total vibrational energy of CO_2 is assumed to be the sum $e_{v_1} + 2e_{v_2} + e_{v_3}$. The diatomic molecule N_2 has only one vibrational mode with ν_i and T_i $(i = 4)$.

Since the rotational relaxation times are very small, the rotational mode is assumed to be in equilibrium with the translation mode so that the rotational temperature is equal to the translational one.

The vibrational energy transfers from N_2 to CO_2 may be expressed with the following processes:

V-T processes:

$$CO_2^*(v_2) + M \rightleftharpoons CO_2 + M + 667 \text{ cm}^{-1}$$

$$N_2^* + M \rightleftharpoons N_2 + M + 2331 \text{ cm}^{-1}$$

V-V processes:

$$CO_2^*(v_3) + N_2 \rightleftharpoons CO_2 + N_2^* + 18 \text{ cm}^{-1}$$

$$CO_2^*(v_3) + M \rightleftharpoons CO_2^{**}(v_2) + M + 416 \text{ cm}^{-1}$$

$$CO_2^*(v_1) + M \rightleftharpoons CO_2^{**}(v_2) + M + 102 \text{ cm}^{-1}$$

In these equations, M represents a collision partner, which may be CO_2, N_2, He, Ar, H_2.

The first reaction in the V-V transfer processes is called the pumping reaction due to the quasiresonant effect between the corresponding energy levels differing only by 18 cm^{-1}.

In the present analysis, we assume, in agreement with Munjee[1] and Losev,[11] that the ν_1 and ν_2 CO_2 modes are in equilibrium with an effective vibrational energy $e_{v_{12}} = e_{v_1} + 2e_{v_2}$ and that $T_{12} = T_1 = T_2$. Thus, only only three modes are present; i.e, modes 12 and 3 for CO_2 and mode 4 for N_2.

The expressions for the source terms $\dot{\omega}_i$ and time rate in the relaxation equations may be obtained from Refs. 10 and 11.

Numerical Method and Boundary Conditions

A finite-difference form of the governing equations is integrated in the nozzles and the cavity of the laser. The chosen numerical method is based on a MacCormack scheme with a time-splitting technique.[6]

Since we are interested only in the steady solution, the integration in time should be carried out until the solution converges to a steady-state one.

At each time step the solution is updated using the following sequence:

$$U^{n+1} = L_y(\Delta t/2) \cdot L_x(\Delta t) \cdot L_y(\Delta t/2) U^n$$

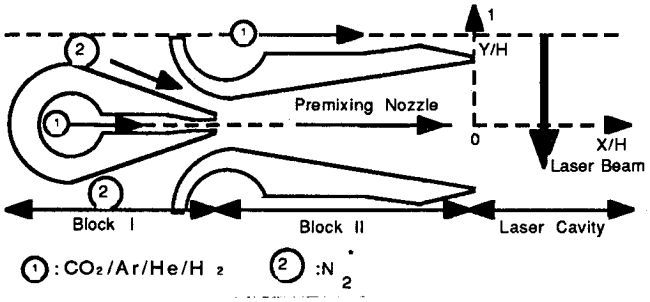

Fig. 1 Schematic diagram of gasdynamic laser.

The vector H, which contains the x derivatives of area and the source terms of relaxation equations, is included in the L_x operator for the numerical treatment.

At each point of the grid system, the integration step time must be lower than the minimum of fluid step time and of the relaxation time of each internal mode.

Four kinds of boundaries are encountered in the computational domain:

1) Solid wall: The velocity components are equal to zero, the pressure is obtained from the second momentum equation, and the normal gradients of temperature, vibrational energy, and species are also taken equal to zero.

2) Symmetry axis: The normal component of the velocity v and the normal gradients of all other unknowns are set equal to zero.

3) Exit boundary: All of the flow quantities along this boundary are extrapolated from the upstream values.

4) Inlet boundary: In the nozzle flow, the parameters are calculated by a method that is decribed in detail in Ref. 12.

In the cavity flow, the quantities are deduced from the calculation nozzle flow and are held constant during the iterations.

Results and Discussion

The arrangement of the nozzles and the computational domain are presented in Fig. 1, taking into account the bank of used nozzles. The flow computation has been decomposed in three parts:

1) The first one is the excited nitrogen nozzle flow with the following reservoir conditions: $P_o = 1$ bar, $T_o = 500$ K, $T_{v_o} = 3000$ K, and the homogeneous mixture $CO_2/He/H_2/Ar$ nozzle flow with respective concentrations 0,32/0,53/0,12/0,03 and reservoir conditions $P_o = 1$ bar and $T_o = 500$ K (block I, upstream nozzles).

2) This first calculation allows us to obtain the flow property profiles at the outlet of the nozzles and, therefore, to calculate the premixed flow of N_2 and CO_2 in the nozzle where the two previous jets are arriving. Then, computing similarly in the nozzles the homogeneous flow of the same mixture

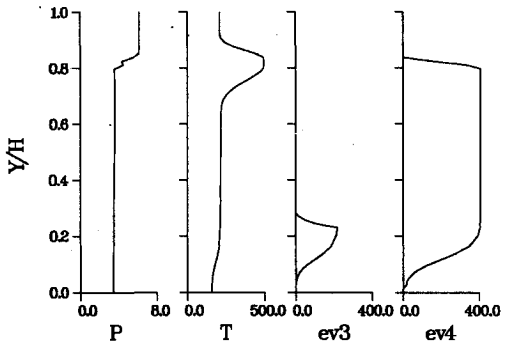

Fig. 2 Transverse profiles as the inlet section of the laser cavity: P (10^{-2} bars), T (K), e_{v_3} (J/g), and e_{v_4} (J/g).

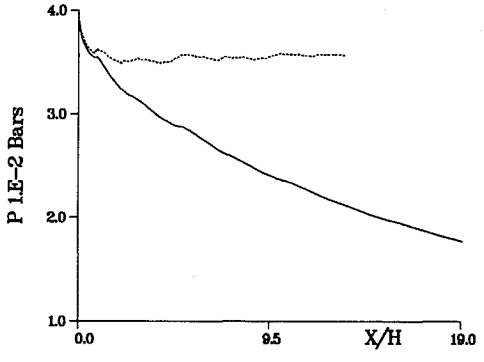

Fig. 4 Variation of average pressure along the laser cavity (---- 0 deg angle, ——5 deg angle).

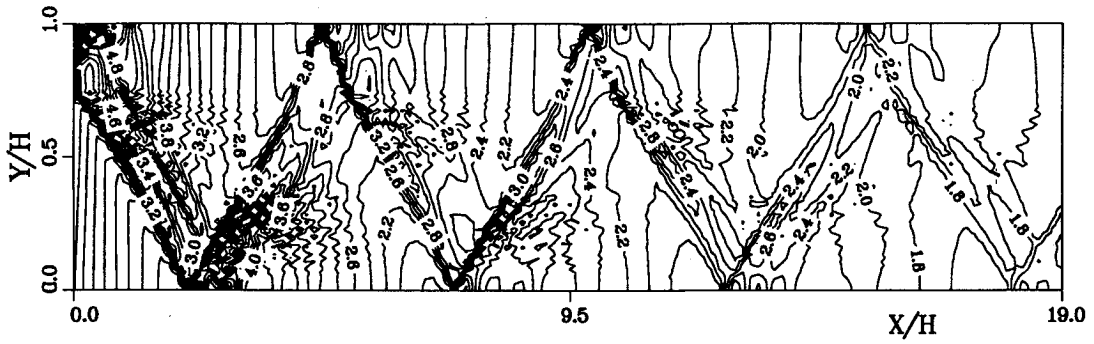

Fig. 3 Distribution of isobar curves (10^{-2} bars) in the laser cavity.

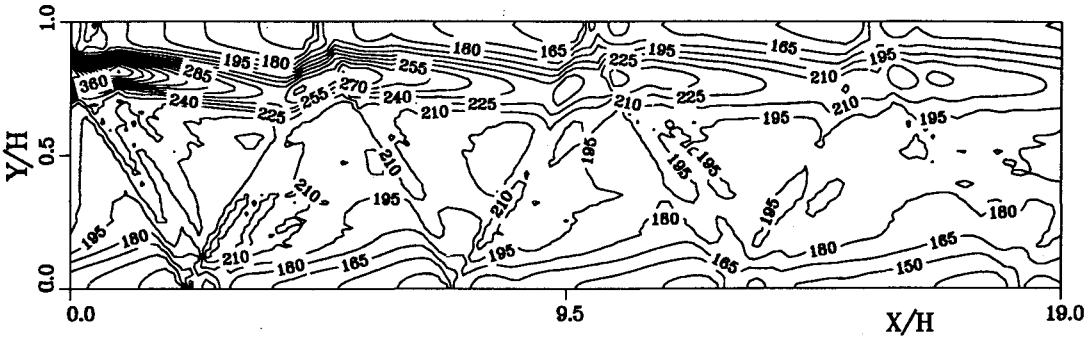

Fig. 5 Distribution of isotherm curves (K) in the laser cavity.

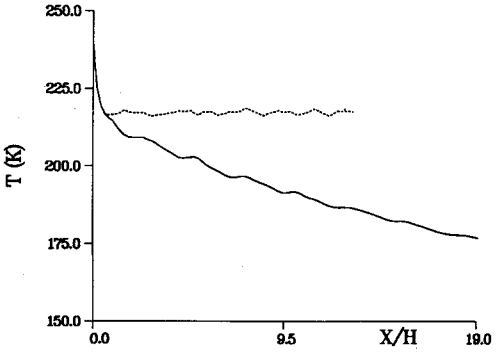

Fig. 6 Variation of average temperature along the laser cavity (---- 0 deg angle, ——5 deg angle).

$CO_2/HE/H_2/Ar$ with the same reservoir conditions (downstream nozzle), the flow in the second part may be determined (block II).

3) As already stated, the profiles at the outlet of the nozzles are taken as inlet conditions ($x = 0$) for the computation of the flow in the laser cavity. In this section, the half heights of the nozzle exit sections are respectively equal to 0.26 and 0.045 cm.

This separation of the flow is, of course, made possible only because of the supersonic regime existing in each part of the arrangement.

A detailed description of the structure of the flowfield in these staggered nozzles may be found in Ref. 10, and only the profiles of pressure, temperature, and vibrational energy of nitrogen and of v_3 mode of CO_2 at the inlet section of the cavity are represented in Fig. 2. A ratio of about 2 may be observed between the outlet pressure values of each nozzle. Thus, the premixing zone between CO_2 and N_2 is responsible of a nonnegligible energy of the v_3 mode of CO_2 level and of a decrease of the N_2 vibrational energy mode. The region of constant vibrational energy for N_2 ($T_v = 2750$ K) constitutes the energetic source during the mixing in the laser cavity with the CO_2 flow mixture of the other nozzle of block II.

Thus, in this cavity, two mixing zones are developing due to this disposal of nozzles allowing the increase of the reactive zone in the laser cavity without reducing the geometrical dimensions too much.

In this cavity, the grid mesh involves (500 × 75) points in the (x,y) plane for the analysis of a length $x/H = 19$ with $H = 0.325$ cm. The wall angle in the z direction is 5 deg from $x/H = 0.77$. The computing time on a CRAY 2 computer is about 10^{-3} s per mesh point and per iteration. The steady solution is obtained after 1500 iterations. The results are presented under the form of isovalues, which are representative of the flow structure, and also under the form of average values along the cavity.

The representation of isobar curves is shown in Fig. 3. The structure of the flow includes oblique shock waves arising at the outlet of the nozzles and reflecting on the symmetry axis. The attenuation of the values of the pressure may be noted along the cavity principally due to the diverging area of this cavity. This effect is also obvious in Fig. 4, which represents the evolution of the average pressure with and without diverging angle. With a zero angle, the pressure remains constant around a value of 35 mbar after the expanding region of the two jets, whereas with a 5 deg angle, a continuous decrease of pressure is observed. This is accompanied by a faster homogenization of the pressure field.

The isotherm curves are represent in Fig. 5. The development of the boundary layers issued from the nozzles are clearly visible as well as their transformation in mixing zones. The impact of compression waves and the decrease of the temperature values are also evident along the cavity. The average temperature goes from 240 K at the nozzle outlets to 175 K at $x/H = 19$ (Fig. 6).

One of the most interesting results concerns the distribution in the cavity of the energy of the v_4 mode of N_2 and of the v_3 mode of CO_2. This distribution is a good picture of the evolution of the two mixing zones and finally of the vibrational transfer between N_2 and CO_2 (Figs. 7 and 8). The steep slope changes of the curves are due to the compression waves crossing the mixing zones. The decrease of the energy available in the excited N_2 may be noted, this being due to the progressive diffusion of CO_2 along the cavity.

In order to have a better insight of the transfers, the transverse profiles of the energies are drawn at different abscissas along the cavity (Figs. 9 and 10), and, for example, it is clear that the nitrogen has completely diffused through the whole section at $x/H = 19$, whereas the CO_2 occupies only three-quarters of this section.

The small-signal gain coefficients are computed easily when the flow is completely known, particularly the average small-signal gains that are experimentally measurable. Thus, for the transition $v_3 \rightarrow v_1$ and for a rotational transition corresponding to the P14 branch (10.6 μm), the evolution of the average small-signal gain coefficient is presented in Fig. 11 for each of

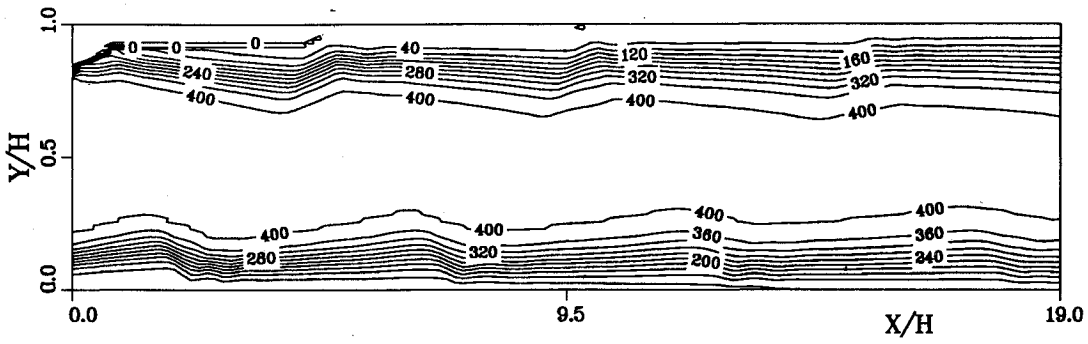

Fig. 7 Isovalue (J/g) profiles of vibrational energy of N_2 in the laser cavity.

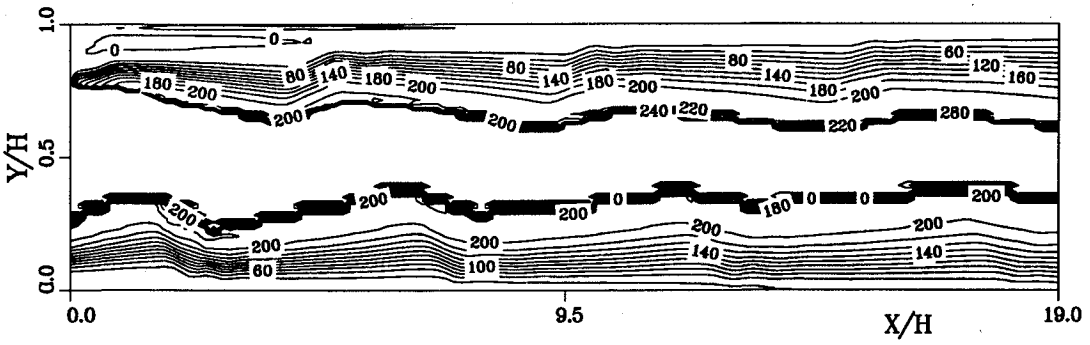

Fig. 8 Isovalue (J/g) profiles of vibrational energy of ν_3 mode of CO_2 in the laser cavity.

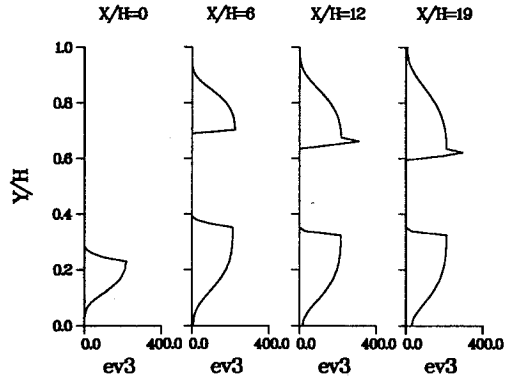

Fig. 9 Transverse profiles of the vibrational energy of ν_3 mode of CO_2 in the laser cavity.

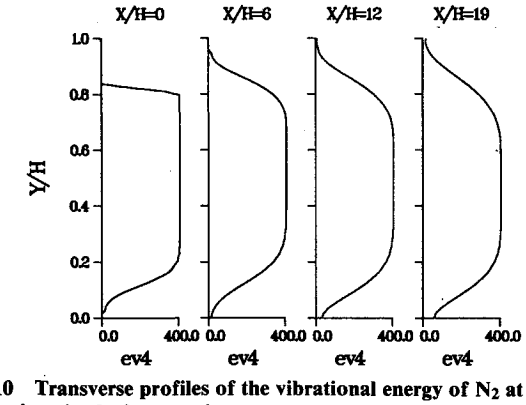

Fig. 10 Transverse profiles of the vibrational energy of N_2 at different sections in the laser cavity.

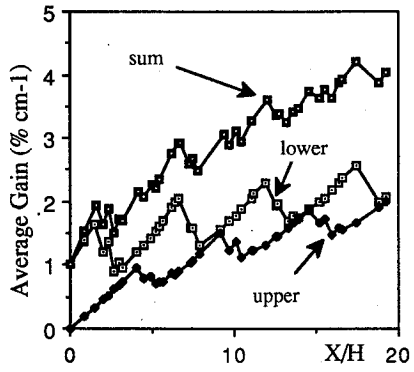

Fig. 11 Variation of average small-signal gain of mixing zones along the laser cavity.

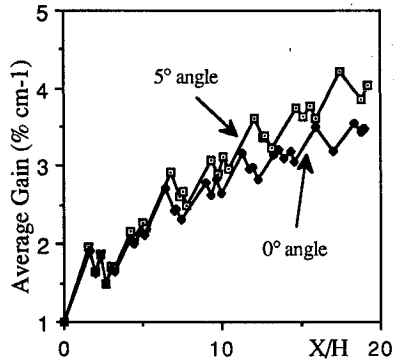

Fig. 12 Variation of average small-signal gain along the laser cavity.

the mixing zones and the total value. It is to be noted that the inlet value is of the order of 1% due to the premixing nozzle. Then, the presence of strong compressions leads to a decrease of the gain. These perturbations are more important in the downstream part of the mixing zone because of the wave reflections. Globally, the gain coefficient becomes greater than 4% cm^{-1} at the end of the computational domain.

At last, the influence of the diverging angle of the cavity on the small-signal gain is represented in Fig. 12. Thus, the area increase is responsible for an increase of the gain of about

13% at the end of the analyzed zone because of the corresponding decrease of temperature and pressure promoting the energetic exchanges between CO_2 and N_2.

Conclusions

From the computation results, the principal following points must be underlined:

1) The boundary layers of the nozzles must be taken into account in order to have a good description of the flowfield in the laser cavity.

2) The small-signal gain value is improved by a premixing of N_2 and CO_2 due to the staggered nozzles.

3) The increase of the area of the cavity leads to an increase of the gain and may be correctly taken into account in a two-dimensional computation.

Acknowledgments

This work was supported by the Direction des Recherches et Etudes Techniques and the Centre de Calcul Vectoriel de la Recherche.

References

[1]Munjee, S. A., "Numerical Analysis of a Gasdynamic Laser Mixture," *Physics of Fluids,* Vol. 15, March 1972, pp. 506-508.

[2]Anderson, J. D., *Gasdynamic Laser: An Introduction,* Academic, New York, 1976, pp. 21-23.

[3]Parthasarathy, K. N., Anderson, J. D., Jr., and Jones, E., "Downstream Mixing Gasdynamic Lasers: A Numerical Solution," *AIAA Journal,* Vol. 17, No. 11, 1979, pp. 1208, 1215.

[4]Fomin, N. A., Solukhin, R. I., Golovichev, V. I., and Munjee, S. A., "Modeling of Gasdynamic and Relaxation Phenomena in Mixed Flow Lasers," *Progress in Aeronautics and Astronautics: Combustion in Reactive System,* Vol. 76, edited by M. Summerfield, AIAA, New York, 1979, pp 46-75.

[5]Chakravarty, P., Reddy, N. M., and Reddy, K. P. J., "Two-Dimensional Analysis of a 16μm CO_2, Downstream-Mixing Gas Dynamic Laser," *AIAA Journal,* Vol. 25, No. 5, 1987, pp. 713-720.

[6]MacCormack, R. W., and Baldwin, B. S., "A Numerical Method for Solving the Navier-Stokes Equations with Application to Shock Boundary Layer Interactions," AIAA Paper 75-1, Jan. 1975.

[7]Zeitoun, D., Imbert, M., Torchin, L., and Brun, R., "Effect on Inlet Pressure on Chemical Laser Flowfield," *Gas Flow and Chemical Laser,* No. 15, edited by S. Rosenwaks, Springer-Verlag, 1987, pp. 29-34.

[8]Wilke, C. R., "A Viscosity Equation for Gas Mixtures," *Journal of Chemical Physics,* Vol. 18, No. 4, 1950, pp. 517-519.

[9]White, F. A., *Viscous Fluid Flow,* McGraw-Hill, New York, 1974, pp. 28-36.

[10]Maurel, M., "Modélisation et Simulation Numérique des Ecoulements de Mélanges Gazeux Hors d'Equilibre Vibrationnel," Thése de Doctorat, Université d'Aix-Marseille 1, France, Jan. 1989.

[11]Losev, S. A., *Gas Dynamic Laser,* Springer Series in Chemical Physic, edited by V. I. Goldanskii, Springer-Verlag, No. 12, 1981, pp. 79-89.

[12]Imbert, M., and Zeitoun, D., "Etude Numérique d'un Ecoulement à Nombre de Reynolds Modéré dans une Tuyére," *Journal de Mécanique Théorique et Appliquée,* Vol. 1, No. 4, 1982, pp. 595-609.